ELSEVIER

Physica C 289 (1997) 230–242

PHYSICA C

Investigation of the evolution of $YBa_2Cu_3O_{7-\delta}$ films deposited by scanning pulsed laser deposition on different substrates

K.H. Wu *, S.P. Chen, J.Y. Juang, T.M. Uen, Y.S. Gou

Institute of Electrophysics, National Chiao-Tung University, Hsinchu, Taiwan 30010

Received 8 May 1997; revised 12 June 1997; accepted 10 July 1997

Abstract

The evolution of surface morphology of $YBa_2Cu_3O_{7-\delta}$ (YBCO) thin films with sequential thickness ranging from 2 to 250 nm on (110) $NdGaO_3$, as-polished and annealed (110) $SrTiO_3$ and (100) MgO substrates has been systematically investigated with atomic force microscopy (AFM) to elucidate the effects of lattice mismatch, pre-annealing treatment and substrate orientation on the growth mechanism of YBCO films. A scanning pulsed laser deposition system, which has been used to produce 50-mm-diameter thin films, allows us to deposit (001) or (103) YBCO films with various thicknesses on separated substrates in a single run under essentially identical deposition conditions. The AFM images show that (001) YBCO films grown on $NdGaO_3$ follow the Stranski–Krastanov (layer then island growth) mode, while films grown on as-polished MgO and on annealed MgO follow the Volmer–Weber (island without layer growth) mode and step–flow mode, respectively. On the other hand, the evolution of (103) YBCO films grown on both as-polished and annealed (110) $SrTiO_3$ substrates reveals the similar step–flow growth along tilt steps, i.e. the growth proceeds with the *c*-axis of YBCO along [100] or [010] directions of substrate. The formations of distinct elongated grains and microcracks in planar view of such films are also discussed. © 1997 Elsevier Science B.V.

Keywords: Pulsed laser deposition; Large area deposition; Film evolution; Substrate effect; (110) $SrTiO_3$

1. Introduction

Understanding the physical mechanisms responsible for the exotic properties manifested by the newly discovered high-T_c superconductors (HTSC) as well as exploiting these properties for potential applications have been among the most challenging issues in this field over the past decade. High-quality epitaxial $YBa_2Cu_3O_{7-\delta}$ (YBCO) films suitable for the above purposes are thus of crucial importance. As is well established [1–3], substrate is one of the key factors for growing epitaxial YBCO films. The degree of lattice and thermal expansion mismatches between the film and substrate, the bonding of the deposited atoms with the substrates, and the surface roughness, cleanliness, orientation, and defects of the substrate can influence the final quality of the deposited films drastically. In order to deposit high quality epitaxial YBCO films in situ, the substrates should be heated up to about 650–850°C during

* Corresponding author. Institute of Electrophysics, National Chiao-Tung University, 1001 Ta Hsueh Rd., Hsinchu, Taiwan 30050. Tel.: +886 3 5712121 ext 56114; Fax: +886 3 5725230; E-mail: khwu@cc.nctu.edu.tw.

PII S0921-4534(97)01608-0

deposition. Therefore, the characteristics of the substrates mentioned above should be discussed in that temperature range. Although the surface peaks of the compositions of substrate surfaces were studied up to deposition temperature by high-temperature Rutherford backscattering spectrometry (RBS) [4], the change of surface morphology has never been observed in situ at high temperatures. However, it was found that the surface morphology and microstructure of the substrates had been changed permanently after heating them up to deposition temperature and these changes could be observed by AFM and measured by XRD after cooling the substrates down to room temperature [5,6]. In addition to the inevitable modification of the substrate conditions, the substrates with grapho-epitaxial treatments such as substrates prepared with artificial surface structure [7], vicinal surface [8,9], plasma cleaning [10], or heat treatment [3,11–13], can also control the nucleation and epitaxial growth of HTSC films.

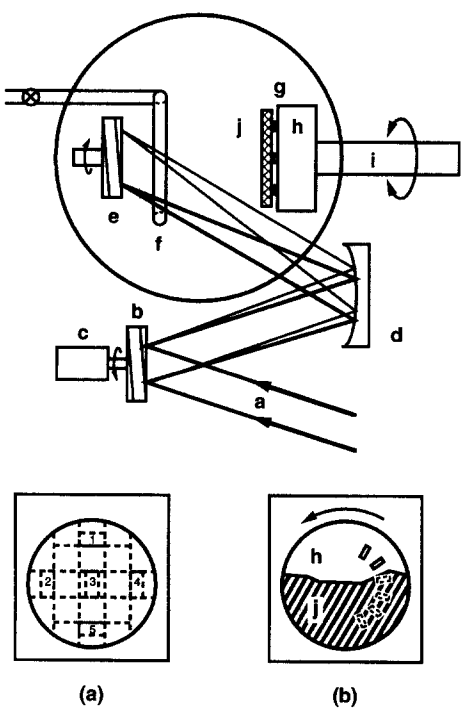

Fig. 1. The schematic diagram of a scanning pulsed laser deposition system. (a) Excimer laser beam, (b) planar reflector, (c) DC motor, (d) concave reflector, (e) YBCO target, (f) oxygen ring, (g) substrate, (h) heater, (i) DC motor, (j) quartz plate. The 50-mm-diameter $LaAlO_3$ was cut into several pieces along the dashed lines in the inset (a) after deposition and the pieces with numbers were further examined the uniformity of the film properties. Inset (b) is the arrangement of substrates for studying the revolution of YBCO films.

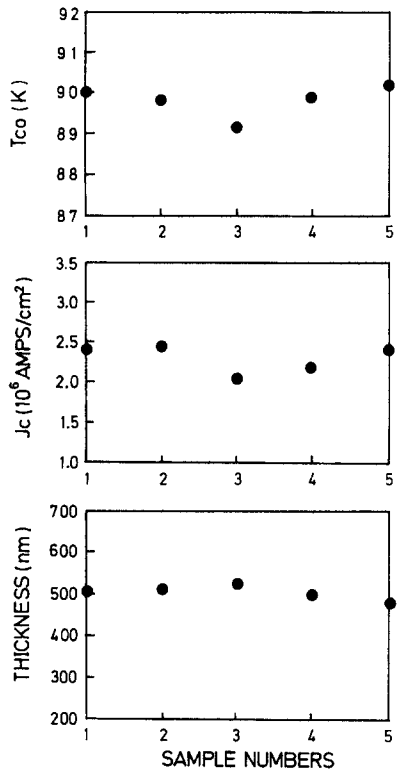

Fig. 2. The uniformity of (a) critical temperature T_{co}, (b) critical current density J_c (at 77 K), and (c) thickness of the YBCO samples with numbers labelled in the inset (a) of Fig. 1.

Many techniques have been used to directly or indirectly probe the growth of YBCO thin films. In-situ resistance measurements [14] and reflection high-energy electron diffraction (RHEED) [15–17] have been used to investigate the interface effects and growth modes for ultrathin film growth. On the other hand, several groups have systematically studied the evolution of YBCO thin films on different substrates by individual deposition [18] or by half-shadow technique [19]. The deposited films were then examined ex-situ by scanning electron microscopy (SEM), transmission electron microscopy (TEM), scanning tunnelling microscopy (STM) or atomic force microscopy (AFM). For the case of ex-situ studies, it is desirable to prepare the films

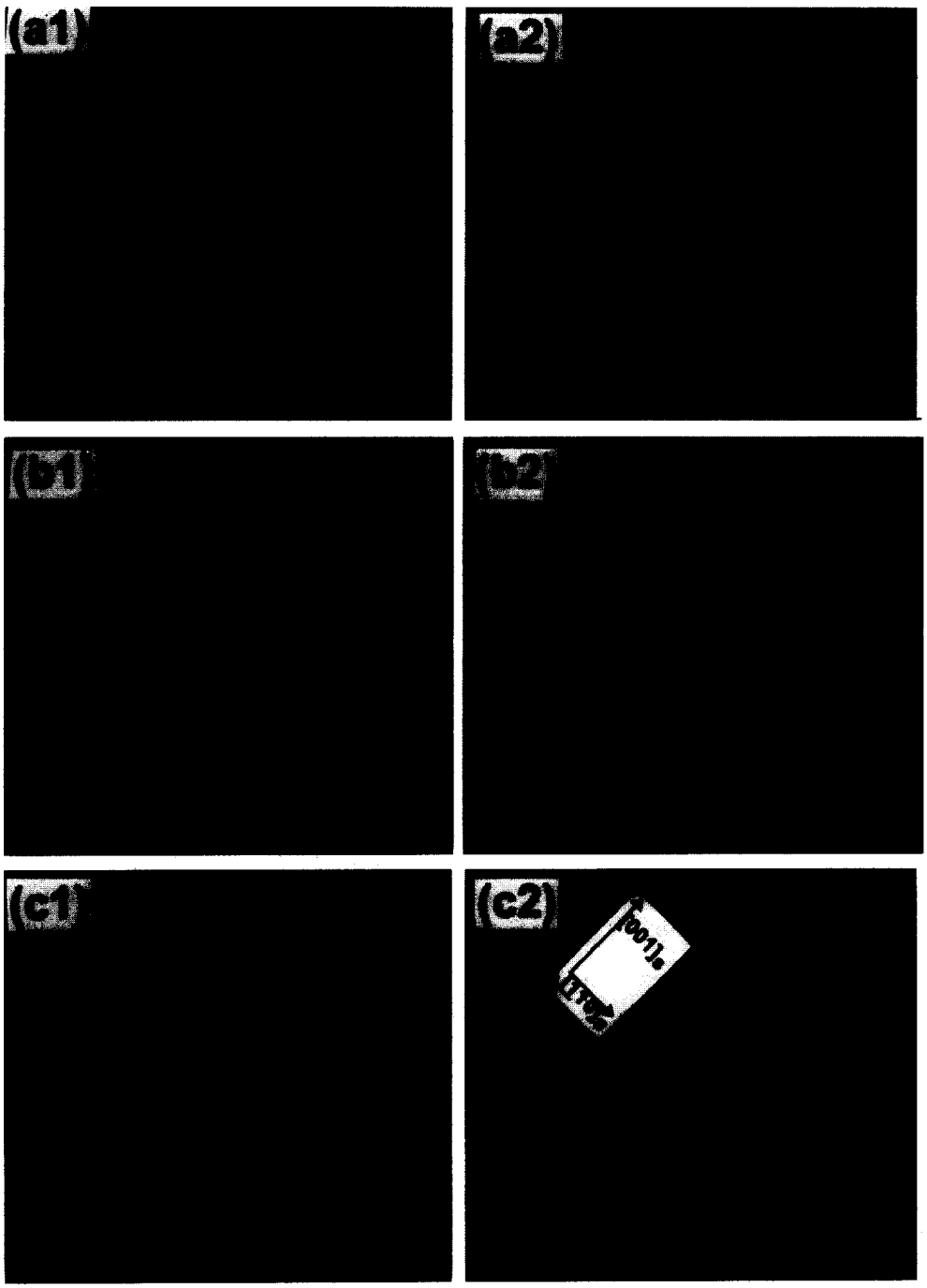

Fig. 3. The substrate surfaces revealed by AFM: (a1) surface of as-polished $NdGaO_3$, (a2) surface of as-polished $NdGaO_3$ after heating at deposition temperature (800°C); (b1) surface of as-polished MgO after heating at 720°C; (b2) surface of MgO after annealing at 1100°C; (c1) surface of as-polished (110) $SrTiO_3$ after heating at 780°C, (c2) surface of $SrTiO_3$ after annealing at 1000°C. The horizontal scales (x, y) are 0.5 μm/division for all the images, and the vertical scales (z) for (a1) and (c1) are 2 nm/division, for (b1), (a2), (b2) and (c2) are 5 nm/division.

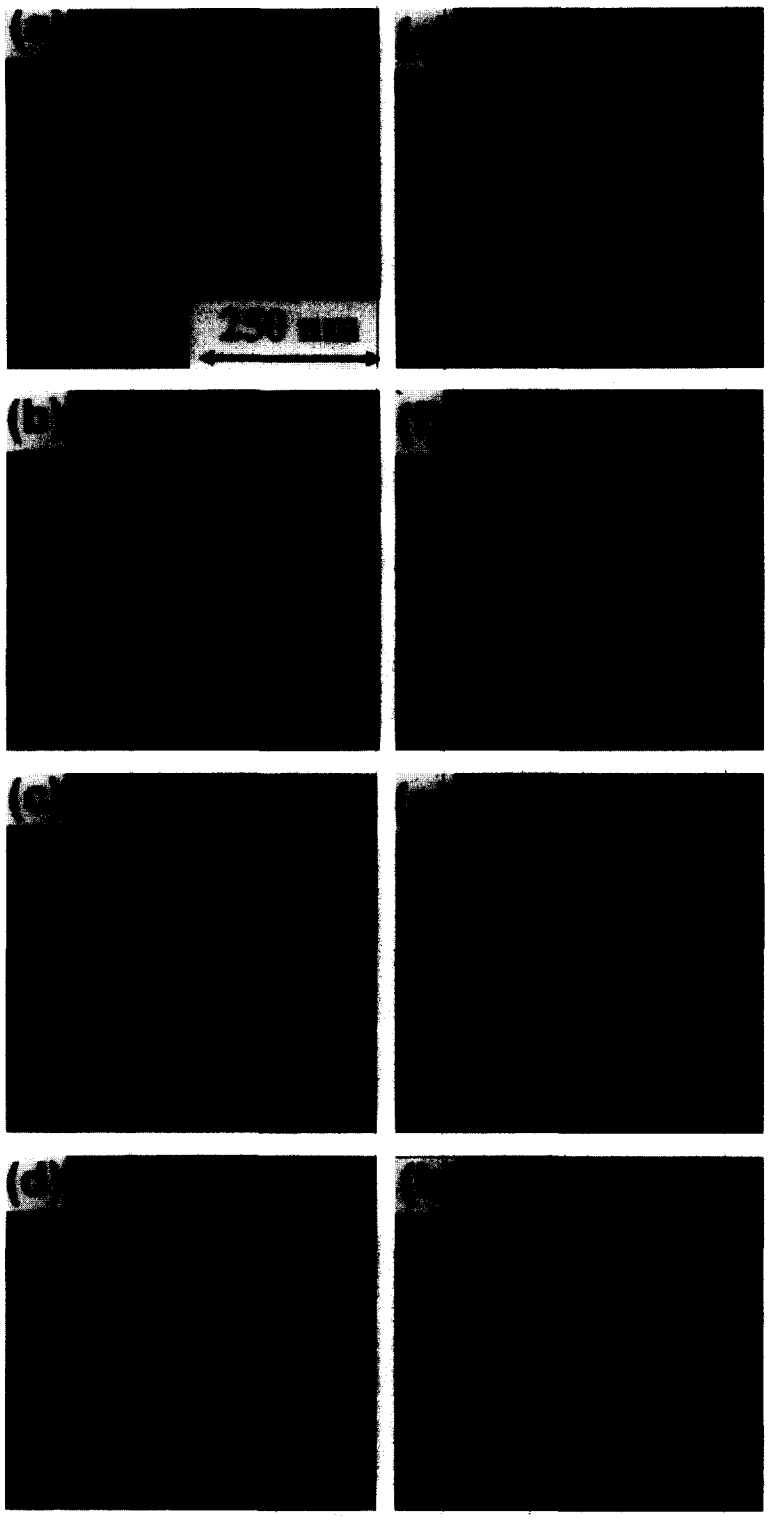

Fig. 4. The AFM images of the YBCO films grown on $NdGaO_3$ with thicknesses (in nm): (a) 2, (b) 5, (c) 10, (d) 30, (e) 50, (f) 100, (g) 150 and (h) 250. All the images are 500×500 nm^2 and the dark-to-light vertical scales for (a) and (b) are 3 nm; (c) to (h) are 5 nm.

with various thicknesses on separated substrates under identical deposition conditions. In the present work, a novel deposition system capable of accomplishing such a goal is reported. A scanning pulsed laser deposition [6] which can prepare YBCO thin films with a diameter of 50 mm has been modified to in-situ deposit films with various thicknesses on separated substrates under essentially identical deposition conditions, and, particularly, in a continuous fashion. These films were then examined by AFM, SEM and STM to delineate the effects of substrate conditions on the growth mechanism of YBCO films at various stages of evolution.

2. Experimental

The scanning pulsed laser ablation system is shown schematically in Fig. 1. A planar reflector and a concave reflector were used to guide and focus the laser beam to a 50-mm-diameter YBCO target situated in the vacuum chamber. Both the planar reflector and the target were rotated by DC motors. There was a small angle between the motor axis and the reflector (or target) axis so that the reflected laser beam scanned a circle prior to impinging on the concave reflector. The focused laser beam then scanned a circle of about 20–30 mm in diameter on the rotating target and generated an extended plume with a diameter of 40–60 mm. A 50-mm-diameter $LaAlO_3$ substrate was attached to a substrate holder assembled with a 50-mm-diameter conventional heater, to obtain a single large area YBCO thin film. The substrate was then cut into several pieces (as shown in Fig. 1a) to test the uniformity of composition, thickness, morphology and superconducting properties of the resultant films over the whole area.

The individual deposition conditions for growing the best optimized (001) YBCO films on (110) $NdGaO_3$ and (100) MgO substrates and (103) YBCO films on (110) $SrTiO_3$ substrate were respectively determined by systematically varying deposition parameters such as laser fluence, repetition rate, substrate temperature, oxygen partial pressure, etc. [20]. Briefly, a KrF excimer laser operating at a repetition rate of 3–8 Hz with an energy density of 2–4 J/cm^2 was used. The partial pressure of oxygen was 250 mtorr. The substrate temperatures, which were monitored by a thermocouple attached to the substrate holder, were kept at 720, 780, 780 and 800°C for films deposited on MgO, $SrTiO_3$, $LaAlO_3$ and $NdGaO_3$, respectively.

However, for studying the evolution of YBCO film during various stages of growth, modifications have to be made. A 50-mm-diameter semi-circular quartz plate, which is shown schematically in the insert (b) of Fig. 1, was installed in front of the heater surface. A 10×10 mm^2 substrate was cut into six pieces. After cleaning or special treatment, the substrates were attached to half of the circular heater surface. The heater can be rotated by a programmable step motor so that the rotational angle can be precisely controlled. Just before deposition commenced, only one substrate was exposed to the target while the others were hidden behind the quartz plate. The heater was then rotated to a presetting angle after a finite time interval of deposition so that the substrate could be exposed to the plume one-by-one. In such a way, films with various thicknesses on separated substrates are obtained during a same deposition run without changing any of the deposition parameters.

Several types of single crystal substrates such as (100) MgO, (110) $NdGaO_3$, (110) $SrTiO_3$ were used for studying the evolution of YBCO film growth. The effects of high-temperature annealing on (100) MgO and (110) $SrTiO_3$ substrates will also be demonstrated. For the annealing process, the cleaned substrates were sealed in a 25-mm-diameter quartz tube. The assembly was first pumped to below 10^{-7} Torr and then filled with 1 atm of oxygen. The temperature was raised to 1000–1100°C and held for 24 h and then slowly cooled with a rate of 2°C/min to room temperature.

3. Experimental results and discussion

3.1. Large area deposition

YBCO films deposited on several pieces of 50-mm-diameter $LaAlO_3$ substrates by the present scanning pulsed laser system, all appeared to be completely black with a mirror-like surface. These films have been used for microwave property measurements and the typical thickness was about 500 nm.

Some substrates have been cut into small pieces to examine the uniformity of the film properties. Fig. 2 shows the uniformity of superconducting critical temperature T_{co} (zero resistance), critical current density J_c (at 77 K) and thickness of five samples located at the $LaAlO_3$ substrate as shown in Fig. 1a. Both the T_{co} and J_c were measured on patterned films by a usual four-probe method. Uniformity with $T_{co} = 89.7 \pm 0.5$ K and $J_c = (2.0\text{–}2.5) \times 10^6$ A/cm^2, and the variation in the film thickness within $\pm 4\%$ were obtained under the optimized deposition conditions. In addition, a conventional θ–2θ X-ray diffraction and scanning electron microscopy analyses also showed that all the films were essentially c-axis oriented and had similar microstructure and surface morphology. The results demonstrate that this system is not only viable for preparing large area YBCO films by pulsed laser deposition, but also is capable of preparing films with different thicknesses under the same deposition conditions.

3.2. Evolution of YBCO films on (110) $NdGaO_3$ substrate

The surface roughness of an as-polished $NdGaO_3$ and a $NdGaO_3$ heated up to 800°C (deposition temperature) then cooled at a rate of 10°C/min to room temperature was revealed by AFM (Nanoscope III, Digital). The three-dimensional view of the images are shown in Fig. 3a1,a2, respectively. It is seen that the surface of the as-polished substrate before heating was atomically smooth with regular ledges along a specific direction. The line-scan profiles reveal the periodic peak to valley (PV) height difference of about 0.5 nm and the root mean square (rms) surface roughness of only 0.2 nm over a distance of 2 μm. The surface after heating became rougher and some extra spikes were occasionally observed. The modification of the surface morphology of the substrate may be attributed to oxygen-deficiency-induced surface reconstruction and impurity contamination resulted from heating the substrate at elevated temperatures and under the vacuum of 10^{-6} torr prior to deposition [4].

The YBCO films with thicknesses of 2, 5, 10, 30, 50, 100, 150 and 250 nm are shown in Fig. 4a–h, respectively. It is noted that the term 'thickness' here is inferred from the numbers of laser pulses delivered. In our deposition conditions, the average deposition rate was estimated to be 0.1 nm per pulse. As is evident from Fig. 4a, for films thinner than 2 nm, there were many smooth nuclei preferentially aligned with respect to the substrate. The average width of the nuclei varied from 70 to 130 nm and the number density was about 10^{10}/cm^2. The surface roughness measured by a three-dimensional view of the AFM image was less than 1.5 nm. The grains at the very early stages will then extend laterally and coalesce regularly and cover the entire substrate surface (Fig. 4b–d) before nucleating the second layer on the first one. This implies that the initial growth of YBCO on $NdGaO_3$ appears to be a two-dimensional (2D) layer growth [21]. This growth mode persisted until the film thickness was increased up to a few tens of nm. However, as the film thickness increased to beyond 50 nm, the growth mode switched to three-dimensional (3D) island growth, as can be seen in Fig. 4e. Irregular clusters of YBCO with various sizes were grown on the top of YBCO grains and formed the terrace structure. The surface roughness abruptly increased to about 6 nm at this stage. After the coalescence of the 3D islands, the surface morphology of the films remains essentially the same as the deposition proceeds to the thickest film (250 nm) examined (Fig. 4f–h).

3.3. Evolution of YBCO films on MgO substrate

The AFM images of the surface morphologies of a MgO heated up to 720°C and a MgO annealed at 1100°C are shown in Fig. 3b1 and b2, respectively. As in the case of $NdGaO_3$, the surface of the as-polished MgO after heating up to deposition temperature became rougher and existed spikes. However, the surface of annealed MgO changed drastically. As shown in Fig. 3b2, unit-cell high steps were densely formed on the substrate surface, which seems to significantly influence the nucleation process of YBCO films. For comparison, the AFM images of the surface morphologies for YBCO films grown on as-polished MgO and annealed MgO are shown in Fig. 5a1–a4 and Fig. 5b1–b4, respectively. As evident from Fig. 5a1–a3, below a film thickness of 50 nm, the evolution of YBCO films grown on as-polished MgO is quite different from those observed in the $NdGaO_3$ case. Randomly oriented grains with

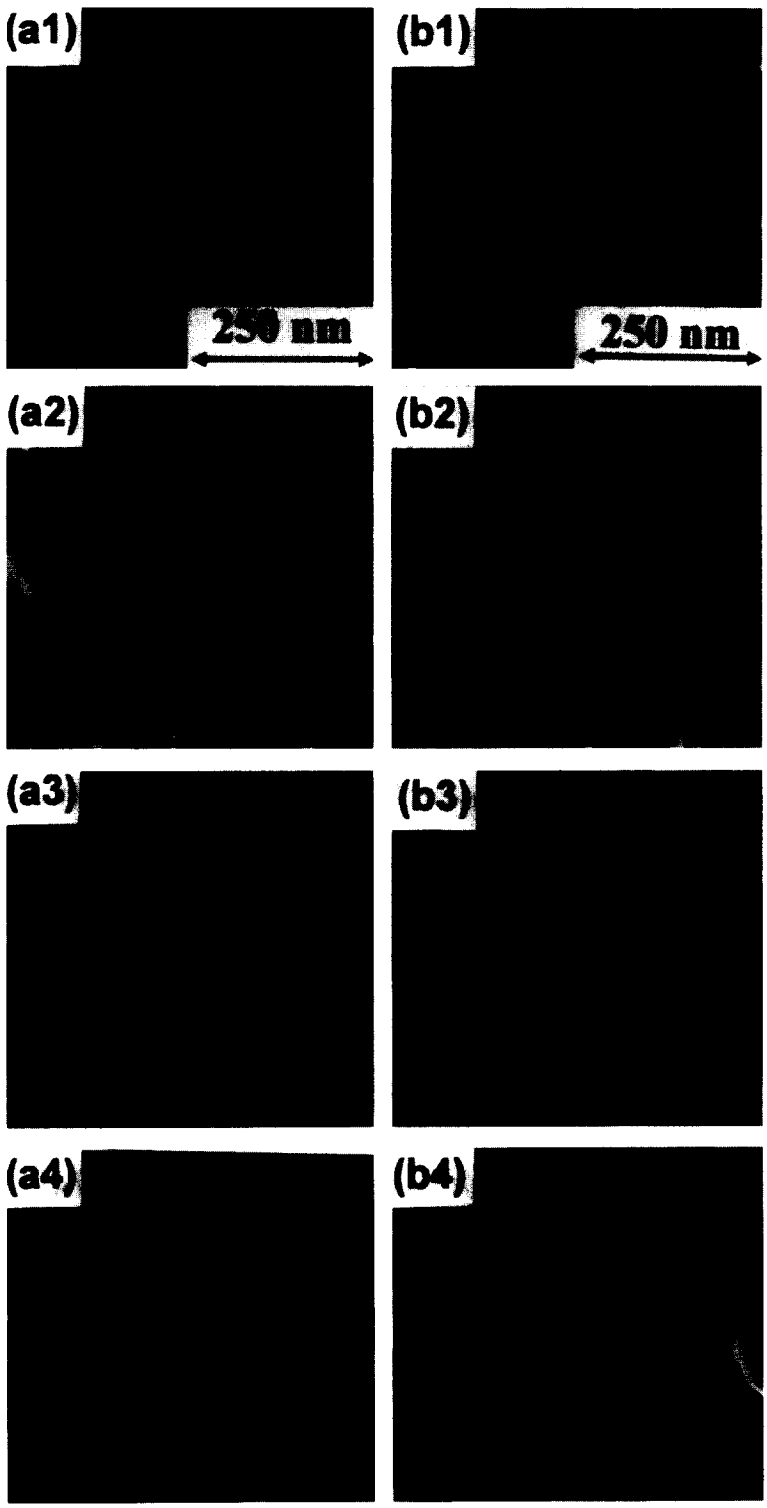

Fig. 5. The AFM images of YBCO films grown on as-polished MgO with thicknesses (in nm): (a1) 3, (a2) 10, (a3) 45 and (a4) 150; and grown on annealed MgO with thicknesses (in nm): (b1) 2, (b2) 15, (b3) 50 and (b4) 150. All the images are 500×500 nm^2 and the dark-to-light vertical scales are 25 nm for (a1) to (a4) and 20 nm for (b1) to (b4).

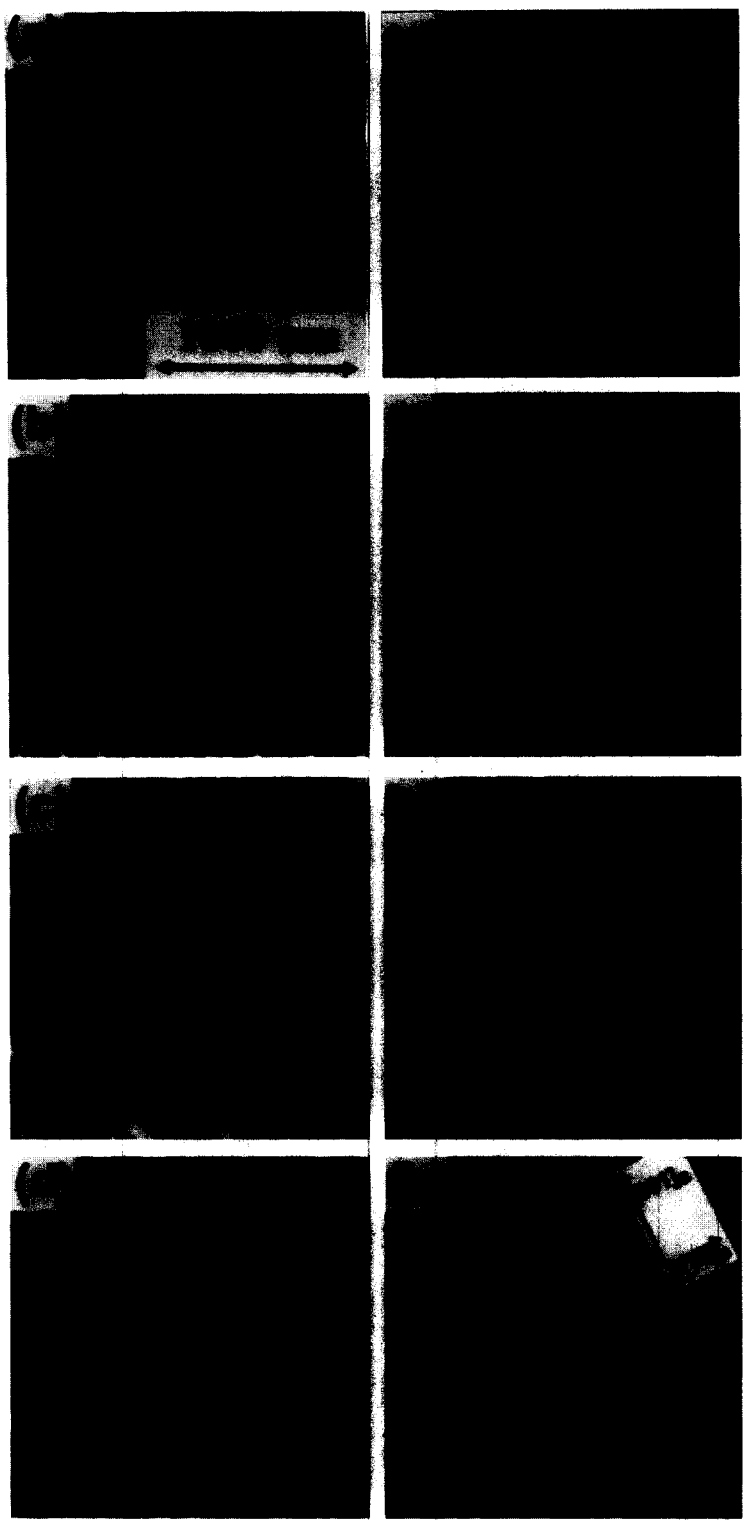

Fig. 6. The AFM images of YBCO films grown on as-polished (110) $SrTiO_3$ with thicknesses (in nm): (a) 2, (b) 5, (c) 10, (d) 60, (e) 100 and (f) 250. All the images are 2×2 μm^2 and the dark-to-light vertical scales are 20 nm.

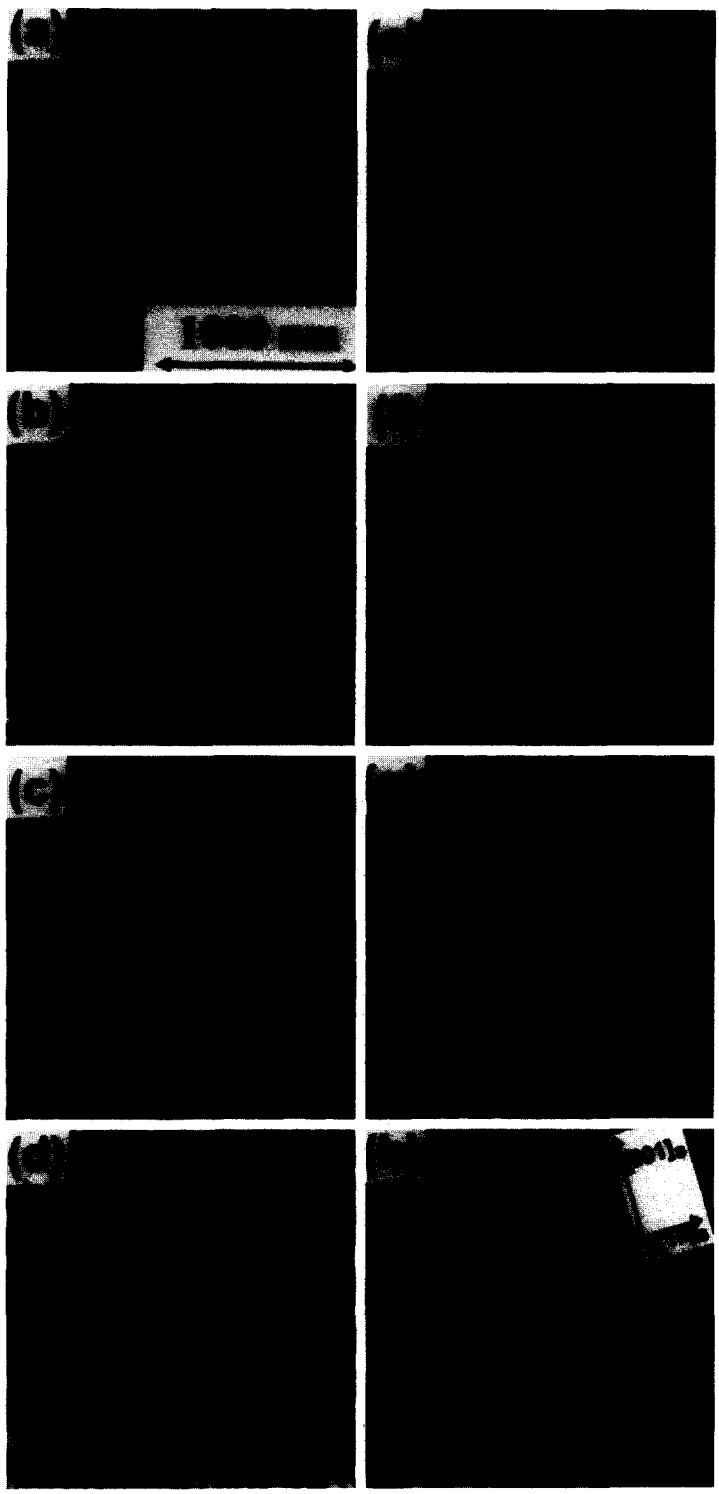

Fig. 7. The AFM images of YBCO films grown on annealed (110) $SrTiO_3$ with thicknesses (in nm): (a) 2, (b) 5, (c) 10, (d) 30, (e) 60, (f) 100, (g) 150 and (h) 250. All the images are 2×2 μm^2 and the dark-to-light vertical scales are 20 nm.

an average dimension varied from 40 to 70 nm were formed and the surface roughness was greater than 3 nm even for a film as thin as 3 nm (average) thick. This indicates that the growth mode of YBCO on as-polished MgO is strictly 3D island growth throughout. As the deposition proceeded, each grain grew independently until merging with the neighbouring grains laterally at a larger thickness, resulting in large individual grain and, occasionally, pinholes at the triangular coalescence regions (Fig. 5a3). After coalescence, the thicker films on MgO showed mosaic texture and disorder structure rather than those grown on $NdGaO_3$.

For YBCO films grown on annealed MgO, as shown in Fig. 5b1–b4, larger grains (85–170 nm) with orderly arrangement or aligned orientation were observed. This is a typical feature of the step–flow growth mode [15,22]. In this case, the edge of steps formed on the annealed substrate are the energetically favourable sites for the nucleation of initial islands. The *a*- and *b*-axes of the films tend to align with the crystal axes of annealed MgO substrate [13]. The surface morphology remained almost the same as the films continued to grow up to 250 nm, indicating that the step density of the step–flow was nearly unchanged. The present results are consistent with the RHEED results reported previously [15], which showed a constant RHEED intensity as a function of time and strong recovery was observed when the deposition is terminated.

The grains nucleated on the edges of steps are expected to have better coherency between neighbouring grains and have a single dominant orientation. This implies that, by treating the substrate properly it is possible to manipulate the growth mode of YBCO films in a controllable manner. The tremendous enhancement in J_c of these films [10,11] is also believed to be closely related to a significant improvement of film microstructure by virtue of annealing the substrates. Therefore, this grapho-epitaxial process may eventually become very important for controlling the quality of (001) YBCO films on MgO suitable for device applications.

3.4. Evolution of (103) YBCO films on (110) $SrTiO_3$ substrate

Films grown on (110) $SrTiO_3$ result in either (103) or (110) YBCO films depending on the deposition temperature and the oxygen pressure [23]. In the present work, we shall study the evolution of (103) YBCO films which were prepared at higher deposition temperature (> 750°C) and lower oxygen pressure (< 250 mtorr). The surface conditions of the (110) $SrTiO_3$ heated up to deposition temperature and annealed at 1000°C are shown in Fig. 3c1,c2, respectively. The surface of (110) $SrTiO_3$ substrate after heating to 780°C was very smooth (Fig. 3c1) while the annealed substrate had high density of steps along $[001]_s$ ([001] substrate direction of (110) $SrTiO_3$) with height of several unit cells (Fig. 3c2).

The schematic view of (103) YBCO films grown on (110) $SrTiO_3$ can be found in refs. [23–26]. Briefly, the *c*-axis of the film is inclined by about 45° out of plane and either parallel to $[100]_s$ or $[010]_s$ axis. The *b*-axis is located in the substrate surface plane and aligns along $[001]_s$ for (103) growth. Therefore, the growth mechanism of (103) films on (110) $SrTiO_3$ along $[\bar{1}10]_s$ direction can be described as an edge or ledge propagation in the *ab*-planes following the initial nuclei on the substrate surface. This type of growth is similar to step–flow growth mode except that the steps are tilted by 45°. Fig. 6a–h and Fig. 7a–h show the detail evolution of (103) YBCO films deposited on as-polished and annealed (110) $SrTiO_3$ substrates, respectively. Since there were no preferential nucleation centres or edges for the smooth as-polished substrates, the nuclei at the early stages were randomly distributed with various sizes (Fig. 6a). On the other hand, more regular alignment of grains with long axis along $[001]_s$ at the initial nucleation for films grown on the annealed substrates was observed (Fig. 7a). As the deposition proceeded, for both cases, the neighbouring grains, grew with the *c*-axis of YBCO along $[100]_s$ or $[010]_s$, interconnected in those directions and formed the triangular structure when viewed from the $[001]_s$ direction. In the meantime, the grains also grew along $[001]_s$ direction rapidly [26] and at the thickness of about 50 nm, the elongated grains would join and cover the whole bare substrates. The width and length of the grains grew continuously as the films got thicker. Since the growth along $[\bar{1}10]_s$ for both cases was very similar to step–flow (with tilt steps) growth mode, thus there were no apparent differences in surface structure for the thicker films grown on as-polished or on annealed (110) $SrTiO_3$ sub-

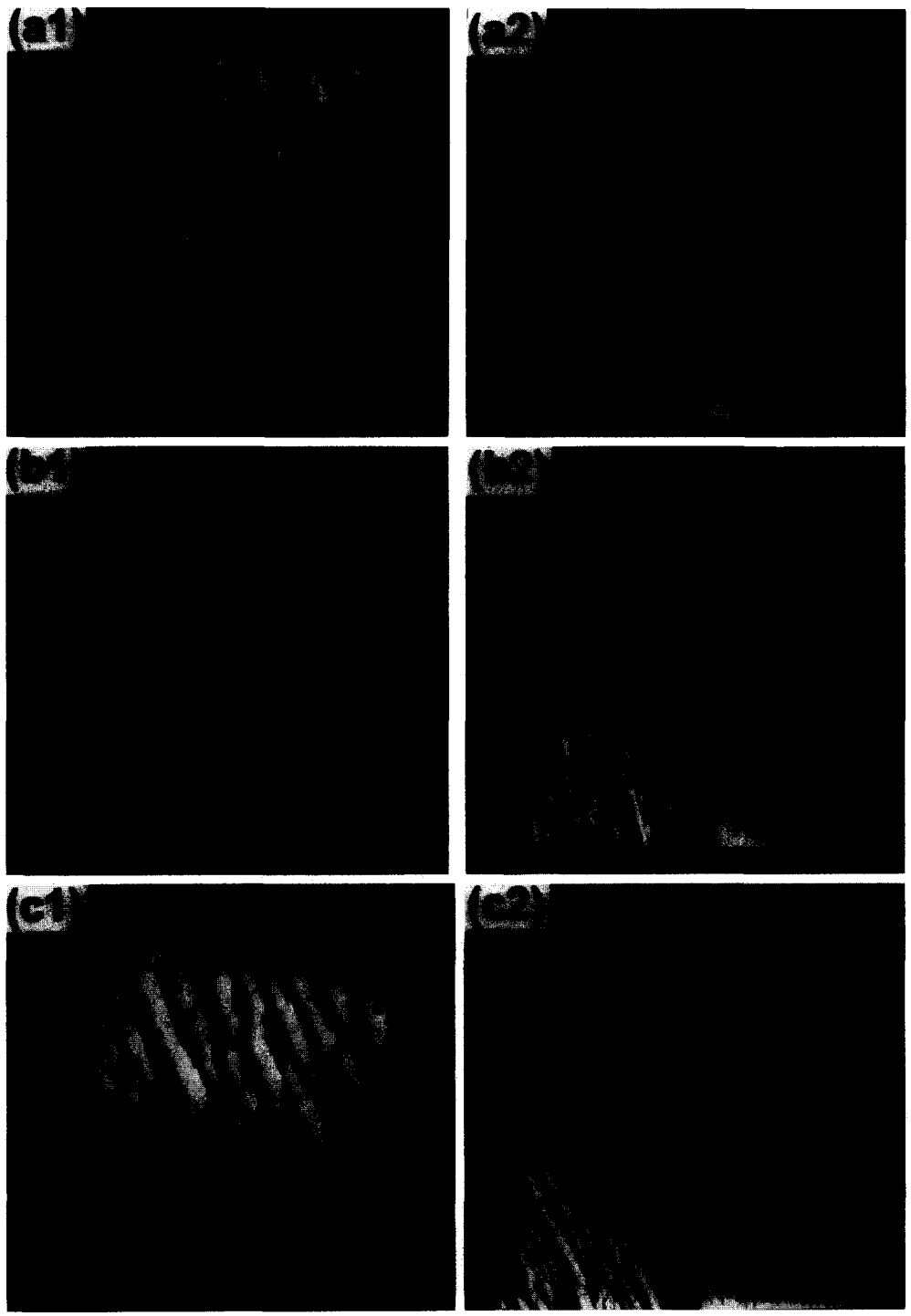

Fig. 8. Three-dimensional view and line scan profile of (103) YBCO film grown on as-polished [(a1) and (a2)] and annealed [(b1) and (b2)] (110) $SrTiO_3$ with a cooling rate of 15°C/min after deposition. The thickness of the film was 250 nm. This cross-sectional view shows the triangular shape structure. (c1) and (c2) show the three-dimensional view and line scan profile of (103) YBCO film grown on as-polished (110) $SrTiO_3$ with a cooling rate of 50°C/min after deposition. The serious cracks were observed even at the thickness of 100 nm.

strates. For both cases, the cross-sectional profile along $[001]_s$ direction shows triangular or saw–tooth structure (Fig. 8a,b) and the height of the corrugation is about 6–8 nm (nearly independent of film thickness as the film thickness is greater than 100 nm). The planar view of the grain structure, however, displayed a distinct 'brick wall' structure with the grain elongated in the $[001]_s$ direction. The length and width of the individual brick at thickness larger than 150 nm remained almost the same and were about 500–1500 nm and 150–250 nm, respectively.

No growth of spirals or terraces, which appeared frequently for the (001) YBCO films, was observed for (103) YBCO films. However, the existence of the domain boundaries and microcracks along both $[001]_s$ and $[\bar{1}10]_s$ directions at thicker films represents the main drawback of the (103) YBCO films. The critical thickness to form the crack depends on the deposition conditions, cooling process and substrate treatment [27]. We found that the critical thickness changed drastically with various cooling rates after deposition. For example, for fast cooling process, namely after deposition the chamber was filled the oxygen to 1 atm and then the substrate was cooled with a rate of 50°C/min to room temperature, serious cracking occurred, as shown in Fig. 8c. On the other hand, if the cooling rate was lower than 15°C/min, no apparent cracks were observed for film thickness of 250 nm on both as-polished and annealed substrates (Fig. 8a,b). Since the surface topology of the (103) YBCO films can influence the physical properties and related junction devices [28], therefore, the causes of the crack formation and how to reduce it should be further investigated. We have measured the transport anisotropies and the pinning behaviours of (103) YBCO films along $[001]_s$ and $[\bar{1}10]_s$ directions and the results will be reported elsewhere.

4. Summary

In this paper the detail evolution of surface morphology of YBCO thin films with sequential thickness ranging from 2 to 250 nm on different substrates has been systematically investigated by AFM. The virtually identical growth conditions in preparing each set of films are realized by the use of a scanning pulsed laser deposition system, which we believed is the most crucial key of making this type of study meaningful.

The AFM images reveal that there are significant differences in the growth mechanisms for the (001)- and (103)-oriented YBCO films. It reveals that the (001) YBCO films grown on $NdGaO_3$ follow the Stranski–Krastanov (layer then island growth) mode. It is 2D nucleation and sequential layer growth at the early stages of growth, then switches to 3D island growth at a critical thickness of 60 nm. The films grown on as-polished MgO follow the Volmer–Weber mode, which means that it is 3D island growth throughout the deposition process, while the films grown on annealed MgO follow the step–flow mode, i.e. islands nucleate at the edge of the preexisting atomic steps on the annealed substrates and grow to form a single dominant orientation. The surface morphology and density of steps remained almost the same for the film thickness up to 250 nm. On the other hand, the growth of (103) YBCO films along $[\bar{1}10]_s$ of (110) $SrTiO_3$ substrate is similar to the tilted step–flow mode and it shows triangular or saw–toothed structure when viewed from the $[001]_s$ direction. Meanwhile, the grains also elongate along $[001]_s$ direction, therefore, the thicker films show the distinct brick wall structure in the planar view. To our knowledge, this is the first time that the grain evolution of (103) YBCO film growth on (110) $SrTiO_3$ substrate has been observed.

Acknowledgements

This work was supported by the National Science Council, Taiwan, under grant No. NSC85-2112-M009-039 and NSC85-2112-M009-035PH.

References

[1] S.K. Streiffer, B.M. Lairson, C.B. Eom, B.M. Clemens, J.C. Bravman, T.H. Geballe, Phys. Rev. B 43 (1991) 13007.
[2] X.Y. Zheng, D.H. Lowndes, S. Zhu, J.D. Budai, R.J. Warmack, Phys. Rev. B 45 (1992) 7584.
[3] M.G. Norton, C.B. Carter, J. Cryst. Growth 110 (1991) 645.
[4] C.C. Chin, T. Morishita, Physica C 245 (1995) 77.
[5] C.C. Chin, T. Morishita, T. Sugimoto, J. Cryst. Growth 132 (1993) 82.

[6] K.H. Wu, R.C. Wang, S.P. Chen, H.C. Lin, J.Y. Juang, T.M. Uen, Y.S. Gou, Appl. Phys. Lett. 69 (1996) 421.
[7] W.D. Dozier, C.E. Platt, Appl. Phys. Lett. 62 (1993) 2048.
[8] B.H. Moeckly, S.E. Russek, D.K. Lathrop, R.A. Buhrrman, M.G. Norton, C.B. Carter, Appl. Phys. Lett. 57 (1990) 2951.
[9] S.K. Streiffer, B.M. Lairson, J.C. Bravman, Appl. Phys. Lett. 57 (1990) 2501.
[10] K.H. Wu, M.H. Li, J.Y. Juang, T.M. Uen, Y.S. Gou, R.T. Kao, Chin. J. Phys. 31 (1993) 1091.
[11] B.H. Moeckly, S.E. Russek, D.K. Lathrop, R.A. Buhrrman, J. Li, J.W. Mayer, Appl. Phys. Lett. 57 (1990) 1687.
[12] E.B. Eom, J.Z. Sun, B.M. Lairson, S.K. Streiffer, A.F. Marshall, K. Yamamoto, Physica C 171 (1991) 354.
[13] M.G. Norton, C.B. Carter, in: S.L. Shindè, D.A. Rudman (Eds.), Interface in High-T_c Superconducting System, Springer, New York, 1994, ch. 1.
[14] W.P. Shen, C. Lehane, J.P. Zheng, H.S. Kwok, Appl. Phys. Lett. 64 (1994) 3175.
[15] T. Frey, C.C. Chi, C.C. Tsuei, T. Shaw, F. Boszo, Phys. Rev. B 49 (1994) 3483.
[16] T. Terashima, Y. Bando, K. Iijima, K. Yamamoto, K. Hirata, K. Hayashi, K. Kamigaki, H. Terauchi, Phys. Rev. Lett. 65 (1990) 2684.
[17] N. Chandrasekhar, V.S. Achutharaman, V. Agrawal, A.M. Goldman, Phys. Rev. B 46 (1992) 8565.
[18] M. Ece, E.G. Gonzalez, H.U. Habermeier, B. Oral, J. Appl. Phys. 77 (1995) 1646.
[19] H.P. Lang, H. Haefke, G. Leemann, H.J. Güntherodt, Physica C 194 (1992) 81.
[20] K.H. Wu, J.Y. Juang, C.L. Lee, T.C. Lai, T.M. Uen, Y.S. Gou, Physica C 195 (1992) 241.
[21] C. Kwon, Q. Li, X.X. Xi, S. Bhattacharya, C. Doughty, T. Venkatesan, H. Zhang, J.W. Lynn, J.L. Peng, Z.Y. Li, N.D. Spencer, K. Feldman, Appl. Phys. Lett. 62 (1993) 1289.
[22] S.J. Pennycook, M.F. Chisholm, D.E. Jesson, R. Feenstra, S. Zhu, X.Y. Zheng, D.J. Lowndes, Physica C 202 (1992) 1.
[23] S. Poelders, R. Auer, G. Linker, R. Smithey, R. Schneider, Physica C 247 (1995) 309.
[24] G. Linker, X.X. Xi, O. Meyer, Q. Li, J. Geerk, Solid State Commun. 69 (1989) 249.
[25] C. Rossel, A. Catana, R.R. Schulz, E.J. Williams, A. Perrin, M.G. Viry, C. Thivet, Physica C 223 (1994) 370.
[26] A.F. Marshall, R. Ramesh, in: S.L. Shindè, D.A. Rudman (Eds.), Interface in High-T_c Superconducting System, Springer, New York, 1994, ch. 3.
[27] E. Olsson, A. Gupta, M.D. Thouless, A. Segmüller, D.R. Clarke, Appl. Phys. Lett. 58 (1991) 1682.
[28] H. Akoh, H. Sato, N. Nakamura, S. Takada, Jpn. J. Appl. Phys. 33 (1994) L766.